ELSEVIER

PII: S0032-3861(97)10103-3

Polymer Vol. 39 No. 20, pp. 4817–4825, 1998

0032-3861/98/$19.00+0.00

Toughening of SAN with acrylic core–shell rubber particles: particle size effect or cross-link density?

A.C. Steenbrink†[a], V.M. Litvinov[b] and R.J. Gaymans[a,*]

[a]*University of Twente, Department of Chemical Engineering, P.O. Box 217, 7500 AE Enschede, The Netherlands*

[b]*DSM Research B.V., P.O. Box 18, 6160 MD Geleen, The Netherlands*

(Received 21 April 1997; revised 24 July 1997; accepted 4 September 1997)

The effect of rubber particle size on fracture toughness and tensile properties have been investigated using styrene–acrylonitrile as a matrix. Pre-formed particles with poly(butyl-acrylate) core and a poly(methyl-methacrylate) shell, ranging from 0.1 to 0.6 μm in diameter, were used as a toughening agent. The morphology was checked by means of transmission electron microscopy. The test methods involved an un-notched uniaxial tensile test, notched Izod impact and notched tensile testing. The experiments were carried out with varying deformation rates and temperatures. N.m.r. experiments were used to measure network densities in the rubber core of the various particles. Uniaxial tensile tests showed that elastic modulus and yield stress of the blends were independent of particle size and network density of the rubber core. There were, however, some differences in cavitation resistance caused by the differences in network density. Easily cavitating particles produced higher toughness in notched Izod impact and notched tensile test but a clear relation with particle size could not be established for the range studied. The brittle–tough transition temperatures were much higher than for materials based on poly(butadiene) core–shell rubbers. It is suggested that the mechanical properties of the rubber particle core are the key to the toughening efficiency. It was found that high toughness could only be achieved if the particles had a low cross-link density (and a corresponding low modulus and low cavitation resistance).

(Keywords: rubber toughening; particle size; cross-link density)

INTRODUCTION

The enhancement of fracture toughness by the incorporation of a rubbery phase in a brittle polymer matrix depends strongly on the mechanical properties of the constituents and the microstructure. Much research has focused on the effect of particle properties on the toughening efficiency for a given matrix material. In particular the influence of particle stiffness, the particle size and the interfacial particle/matrix adhesion has been discussed by numerous authors (see e.g. Refs. [1–4]). Quantification of the separate effects of these variables has often posed experimental difficulties, and a conclusive theory to explain these effects has not been established. For example, the microstructure of the blend is quite sensitive for the processing conditions and the properties of the constituents. In rubber-toughened polystyrene a variation of the fraction of glassy sub-inclusions in the particles for different particle sizes was mentioned by Bucknall *et al.*[5]. This leads to a variation of the volume fraction of composite particles, for the same amount of rubber. Borggreve and Gaymans[6] studied the effect of interfacial adhesion between an EPDM-rubber and a nylon-6 matrix, but noted that the coupling agent also affects the blending process and consequently the particle size. To resolve this problem, the processing conditions had to be manipulated. Seo *et al.*[7] pointed out that cross-linking of the rubber phase has consequences for the viscosity during processing, and thus affects the particle size also. Due to the strong interaction of the various parameters, one must be very cautious when comparing results of different studies.

For rubber-toughened polystyrene (usually containing rubber particles with glassy subinclusions) the optimum particle size is in the order of 1–2 μm. Early theories suggested that the crazing process is affected by the rubber particle size[1–3]. Based on observations on thin films, Donald and Kramer[2] suggested that particles smaller than 0.2 μm are too small to initiate crazes. Solid core–shell particles as small as 0.1 μm can be effective toughening agents for SAN[9] and PVC[10]. Post-mortem electron microscopy of deformed bulk samples showed extensive crazing around the small rubber particles.

A key step in the deformation process is cavitation of the rubber particles. The term 'cavitation' is used here to indicate the processes of initiation and growth of voids inside the rubber particles, possibly caused by an intrinsic material instability or other means of failure mechanisms. This seems to be a generic feature in the deformation behaviour for a wide range of rubber-toughened polymers; cavitation of the rubber particles has been observed both in amorphous[11,12] and semi-crystalline polymers[13–15], as well as in thermosets[16].

In recent studies, the reduced toughening efficiency of small particles is attributed to the increased cavitation

* To whom correspondence should be addressed
† Present address. Delft University of Technology, Laboratory for Engineering Mechanics, Mekelweg 2, 2628 CD Delft, The Netherlands.

Table 1 Designation and particle size and of impact modifiers

Code	Supplier	Diameter (nm)	Shell thickness (nm)	Trade name
RH100	Rohm & Haas	100	unknown	KM 355
RH300	Rohm & Haas	300	5–17	EXL 3300
RH600	Rohm & Haas	600	10–30	EXL 3330
UM150	UMIST	150	10	
UM250	UMIST	250	10	
UM350	UMIST	350	10	
UM450	UMIST	450	15	

resistance, if the rubber particle size is very small[14,15]. For particles smaller than roughly 0.1 μm, the surface tension acting inside the void may have a significant contribution to the cavitation resistance[17]. This results in an increased hydrostatic stress in the matrix which obstructs plasticity and, in turn, leads to a reduction in overall fracture toughness.

The use of pre-formed particles may provide a solution to the aforementioned experimental difficulties, as it enables the properties, size and microstructure of the particles to be pre-defined and unaffected by processing. This paper discusses the effects of various pre-formed rubber particles as a toughening agent for a styrene–acrylonitrile copolymer. The particles consist of a lightly cross-linked butylacrylate core and PMMA shell. Both cross-link density of the rubber core and the particle size are varied.

EXPERIMENTAL

Materials and specimen preparation

Blends of a styrene–acrylonitrile copolymer (TYRIL 790, supplied by the Dow Chemical Co.; acrylonitrile content, 29%) and various acrylic core–shell rubbers were prepared in a Berstorff ZE 25 co-rotating twin screw extruder. Rohm & Haas (RH) supplied Paraloid impact modifiers. Another series of similar particles were prepared at UMIST Manchester (UM). The rubber particles consist of a poly(butylacrylate) (BA) core and a poly(methylmethacrylate) (PMMA) shell. The dynamic modulus and loss factor of the blends have been measured with a Myrenne torsion pendulum at 1 Hz. For all blends the glass transition temperature, T_g, was independent of the composition and was found to be 105°C and −45°C for SAN and BA, respectively. Other properties are given in *Table 1*. The particles are designated with the supplier's name (either RH or UM) and the size in nm; e.g. core–shell particles supplied by UMIST Manchester, with a diameter of 150 nm, are indicated as UM150 particles.

Blends were prepared with the rubber content varying from 20% to 50% mass. Mass densities ρ for both SAN and BA are 1.08×10^3 kg m^{-3}[18,19]. In the sequel, blends will be indicated as follows: matrix/modifier (volume fraction). For example, a SAN matrix containing 20% volume fraction of RH300 particles is referred to as SAN/RH300(20%).

Test specimens were injection moulded and, if appropriate, a 2 mm deep notch with a notch radius of 0.25 mm was sawed into the specimen (*Figure 1*).

Microscopy

Morphology of undeformed test specimens and deformation zones were studied by means of transmission electron microscopy. Samples were trimmed and polished with a glass knife at room temperature on a CryoNova microtome. Thin sections (about 200 nm) were cut with a wet diamond knife using a 50/50 mixture of DMSO/H_2O. The temperature of both chamber and specimen was between −80 and −60°C. The temperature of the bath was −45 to −40°C, close to the freezing point of the solution. The samples were stained in a vapour of rutheniumtetraoxide RuO_4[20].

Proton, solid-state n.m.r. measurements and data analysis

The proton transverse magnetization decays (T_2 relaxation decays) were measured on a Bruker Minispec PC-120 spectrometer at a proton resonance frequency of 20 MHz. This spectrometer was equipped with a home-built, variable temperature unit. Dry nitrogen was used for heating of samples. The temperature gradient and stability is about 1 K.

The T_2 relaxation decays for the rubbery phase were measured by the Hahn-echo pulse sequence, HEPS: 90_x°–τ–180_x°–τ–(acquisition)[21]. The second pulse in HEPS inverts nuclear spins in a soft region of a sample and an echo signal is formed with a maximum at time 2τ after the first pulse. By varying the pulse spacing τ in HEPS, the amplitude of the transverse magnetization was measured as a function of time 2τ. Usually, 70 values of $A(2\tau)$ were measured in the time interval 2τ from 0.07 to 130 ms. The nuclear magnetization from rigid materials is not detected by HEPS[21].

The time constant, T_2, which characterises the slope of the magnetization decay curve, was obtained by performing a least-squares fitting analysis of the data using several decay functions, such as an exponential function, the Kohlrausch–Williams–Watts stretched exponential function, a normal or a log-normal distribution of exponents. The statistically most relevant results were obtained for the exponential decay function:

$$A(2\tau) = A(0)\exp(-2\tau/T_2) \quad (1)$$

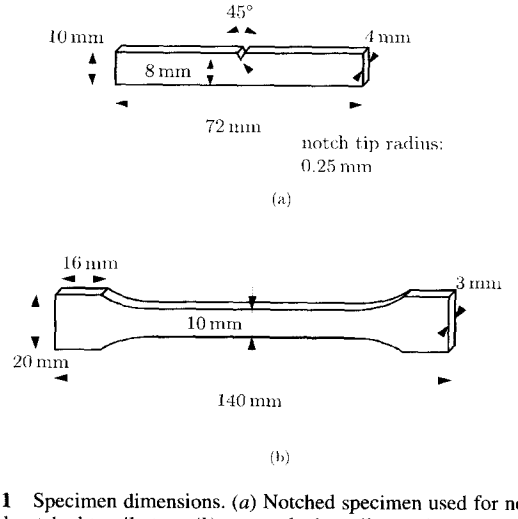

Figure 1 Specimen dimensions. (*a*) Notched specimen used for notched Izod and notched tensile test; (*b*) un-notched tensile specimen

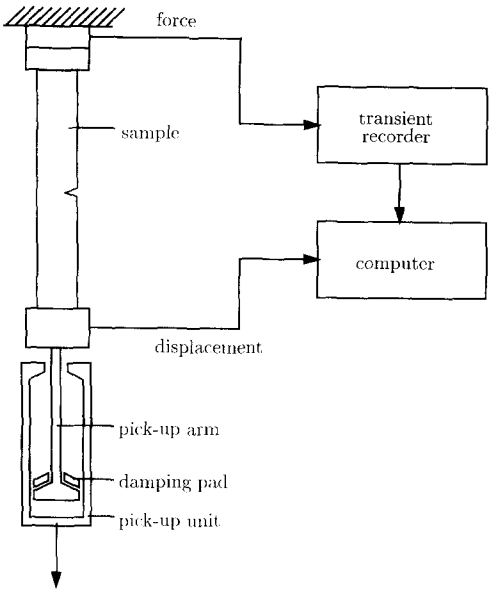

Figure 2 Experimental set-up of the Schenck VHS tensile tester

where $A(0)$ is the equilibrium value of the transverse magnetization.

Selective analysis of the network density in the rubbery phase of immiscible polymer blends by the n.m.r. method

Soft and hard components of immiscible polymer blends can be studied selectively by means of a proton T_2 relaxation experiment[22]. At temperatures which are intermediate between the glass transition for soft and hard phases, T_2 for the soft phase is significantly longer compared to that for the hard phase. Therefore, T_2 values for the rubbery phase in the blends can be measured selectively with a high accuracy.

The T_2 value can be quantitatively related to the network density in crosslinked rubbers[23,24]. At temperatures $T \geq T_g + 150$ K, the temperature dependence of T_2 for vulcanizates has a plateau. The temperature independence of the T_2 value at temperatures well above T_g is attributed to constraints which limit the amount of possible conformations of the network chain with respect to those of a free chain. In other words, due to fast segmental mobility, the network chain takes a conformational mean position which depends on the number of statistical segments between network junctions. In this case, the T_2 relaxation time is determined only by the residual proton dipole–dipole interactions and does not depend on the frequency and type of chain motions. It was found that temporary and trapped chain entanglements contribute to the network density as measured by the n.m.r. method[25].

For Gaussian chains, the number of statistical segments Z between network junctions is calculated from the T_2 value at the plateau (T_2^p), using the following equation[23,24]

$$Z = T_2^p/(aT_2^{rl}), \quad (2)$$

where a is the theory coefficient (for elastomers containing aliphatic protons in the main chain, the coefficient a is close to 6.2 ± 0.7[24]; T_2^{rl} is the relaxation time in the glassy state.

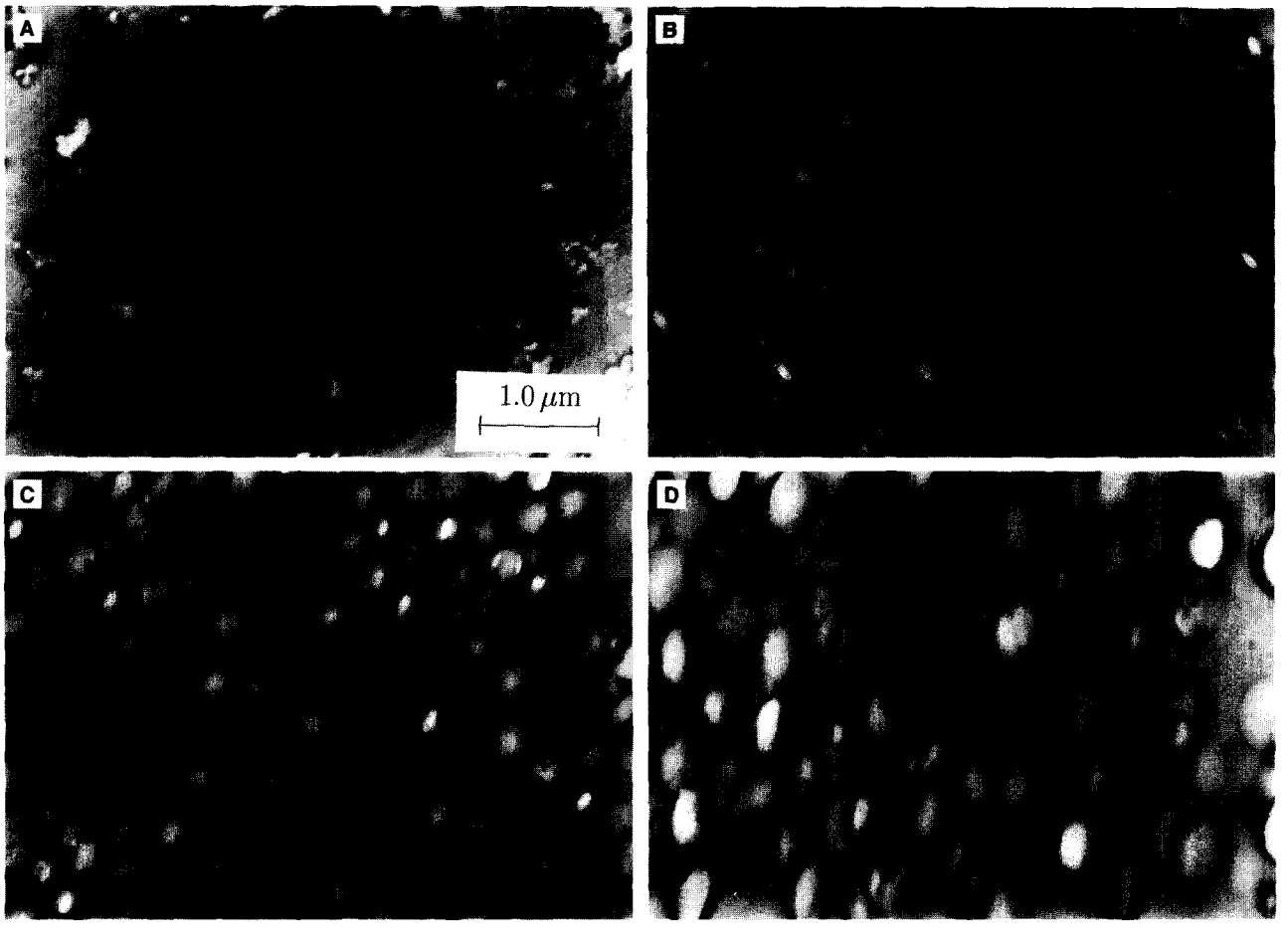

Figure 3 TEM micrographs of undeformed SAN/BA(25%) core–shell rubber blends. (*a*) SAN/UM150, (*b*) SAN/UM350, (*c*) SAN/UM450, (*d*) SAN/RH600

Table 2 Temperature dependence of the T_2 relaxation time (in milliseconds) for BA rubber in the PMMA/BA samples

T (K)	UM450	RH300
333	0.54 ± 0.01	1.25 ± 0.01
353	0.60 ± 0.01	1.54 ± 0.02
363	0.61 ± 0.01	1.64 ± 0.02
373	0.62 ± 0.01	1.73 ± 0.02

Using the number of backbone bonds, C_∞, in the statistical segment, the density of chemical cross-links and chain entanglements is calculated from

$$(2M_{c+e})^{-1} = n/(2ZC_\infty M_u) \quad (3)$$

where M_u is the molar mass per the elementary chain unit and n is the number of rotatable backbone bonds in the elementary chain unit.

Mechanical test methods

The notched Izod test provides a widespread and simple means to measure fracture toughness of samples in a wide range of temperatures. The method is used here to detect transitions in fracture behaviour of the blends between −40 and 80°C.

The tensile test on notched specimens provides similar results, but allows for a more detailed analysis, since the complete force and displacement record is stored. Moreover, it is possible to conduct experiments in a wide range of deformation rates and temperatures. It is crucial that in the high-speed regime special precautions are taken to prevent interference due to internal vibrations[26]. The Schenck VHS servo-hydraulic tensile tester (*Figure 2*) is designed to perform tensile experiments in a speed range from 10^{-5} to 10 m s^{-1}. The piston has a pick-up unit with damped contact at the lower clamp to allow fast acceleration of the specimen, without transmitting severe oscillations. A piezo force transducer is placed at the upper clamp. Force, displacement and time signals are stored in a 2 Mhz Adam Scope transient recorder. The fracture energy is calculated from the force–displacement signals.

Un-notched specimen were used to perform uniaxial tensile tests, from which the Young's modulus and the yield stress are determined. The modulus was computed from the initial slope of the force–displacement curve. Since the tensile specimen is not prismatic, this effect was taken into account using a simplified (small strain) analysis, where the specimen is replaced by a prismatic bar of equivalent stiffness. This leads to the definition of an effective specimen length, which is $L_{eff} = 101.4$ mm. Accordingly, at a tensile speed of 1 m s^{-1} the strain rate is $\dot{\epsilon} \approx 10$ s^{-1}. At larger strains, the slope of the force–displacement curve falls to zero, which is defined as the yield point. The yield stress is defined here as the force at the yield point per unit area of the undeformed geometry ($A_0 = 30$ mm^2).

Cavitation of the rubber particles is detected with a method introduced by Dijkstra *et al.*[15]. A decrease in laser light transmission through an unnotched tensile specimen is taken as the instant of cavitation. This method is suitable even at very high loading rates.

RESULTS AND DISCUSSION

Morphology

The undeformed materials were studied by means of transmission electron microscopy (TEM) in order to determine the particle size, microstructure and possible damage of the microscopy samples by the preparation method. The structure of undeformed material is shown in *Figure 3*. Particle sizes are found to be in close agreement with the manufacturer's indications. Particle size distributions are extremely narrow. The samples containing two smallest particles sizes, RH100 and UM150, show severe clustering (*Figure 3a*) and these batches were therefore excluded from further experiments. The materials with larger particles have a better spatial distribution, although it is noted that they are often aligned in 'chains' rather than isolated in the matrix (*Figure 3b–d*).

One might question whether the interfacial interaction between the SAN matrix and the PMMA shell is good enough to prevent debonding of the particles. In blends which have a serious compatibility misfit the particles would be arranged in agglomerates. This was shown, for example, by Kim *et al.*[28] for SAN/PB blends, where the rubber-graft and the SAN-matrix were immiscible due to the difference in AN content. Here, the particles are quite well distributed in the matrix, suggesting a good interfacial interaction.

The particles are seen in *Figure 3* to be slightly elongated perpendicular to the cutting direction. Due to the high viscosity of the bath, the sections were slightly compressed. Also a fraction of the particles has cavitated during preparation of the microscopy specimen. These cavities are formed mainly inside the rubber particles, indicating that the adhesion between the two phases is good. Also in deformed specimens (not shown here), cavities are found predominantly inside the rubber particles.

N.m.r. experiments

The T_2 relaxation time for the rubber phase in UM450 and RH300 particles is shown as a function of temperature in *Table 2*. Above 350 K, T_2 for UM450 reaches a nearly constant plateau value, T_2^p. The T_2 value for the RH300 sample increases slightly with increasing temperature. This increase is possibly caused by the presence of a significant fraction of network defects: chains which are not attached to the network, dandling chain-ends and chain loops.

The T_2 relaxation time at 373 K for BA rubber in the samples is shown in *Table 3*. It is seen that the T_2^p value for UM samples does not depend on the diameter of core–shell particles and is about three times shorter compared to those for RH samples. The network density composed of chemical cross-links and chain entanglements, $(2M_{c+e})^{-1}$, in BA rubber is estimated from equation (2) and equation (3) for a value of $C_\infty = 8.3 \pm 1$[27] and $T_2^l = 16.4 \pm 0.5$ μs. The values of $(2M_{c+e})^{-1}$ obtained are given in *Table 3*.

Table 3 The T_2^p relaxation time at 373 K and estimated density of chemical cross-links[a] and chain entanglements in BA rubber of PMMA/BA samples

Sample	RH300	RH600	UM250	UM350	UM450
T_2^p (ms)	1.73 ± 0.02	1.77 ± 0.02	0.63 ± 0.02	0.62 ± 0.02	0.62 ± 0.02
$(2M_{c+e})^{-1}$ (mmol kg^{-1})	55	55	150	150	150

[a]The relative error of the network density is estimated to be about 50%. This error is mainly caused by the inaccuracy of coefficients a and C_∞

The absolute error in the network density is estimated to be about 50%. This error is mainly caused by the inaccuracy of the coefficients a and C_∞. Because the chemical structure of all samples is the same, the relative error between the samples involves only the experimental error in the relaxation time (about 2%). Therefore, to a very good accuracy, it can be stated that the rubber network density of the UM particles is a factor of 3 higher than for RH particles.

In order to estimate the shear modulus of the rubber particles, we use the network elasticity theory for Gaussian chains. Accordingly, the relation between mean molecular mass between network junctions M_{c+e} and shear modulus G is given by

$$G = nRT = \frac{2}{fM_{c+e}}\rho RT, \tag{4}$$

where n is network density (mol m^{-3}), R is the universal gas constant (J mol^{-1} K^{-1}] and T is the absolute temperature (K). For the functionality of network junctions, f, a value of 4 is taken. The contribution of chain entanglements to the modulus depends on temperature and loading rate. Because of the relatively fast deformation rate at impact tests, it is assumed that both temporary and trapped chain entanglements contribute to the modulus. The estimated shear modulus for the rubber core of the RH particles at 373 K, according to equation (4), is $G = 0.2$ MPa. For the UM particles we find accordingly $G = 0.6$ MPa. It is emphasized again that the absolute value of the shear modulus is only a rough approximation due to the underlying assumptions, though the results relative to each other are quite accurate.

Tensile test

Effect of volume fraction of RH300 particles on tensile properties. The Young's modulus as a function of rubber content for SAN/RH300 blends, at various strain rates, is shown in *Figure 4*. The modulus decreases linearly with increasing rubber content, and the rate-dependence appears to be very small. This is consistent with the statement that at room temperature and low stresses the relaxation processes are negligible in the time scale of the experiments described here.

A simple theoretical upper bound for the bulk and shear moduli, K and G, respectively, of the heterogeneous material was proposed by Voigt, assuming uniform strain. This yields for blends

$$K_{blend} = (1-\varphi)K_{san} + \varphi K_{ba}, \quad G_{blend} = (1-\varphi)G_{san} + \varphi G_{ba}, \tag{5}$$

where φ is the volume fraction of particles. In general, the Voigt estimate of Young's modulus does not follow from a simple weighting of the volume fractions of the two components (see Ref. [29]), but the difference is not large here, since the shear modulus of the rubber phase is very small compared to the shear modulus of the matrix. Thus, an accurate approximation of the upper bound for Young's modulus E is given by

$$E_{blend} = (1-\varphi)E_{san} \tag{6}$$

It is noted that the experimental data agree accurately to equation (6) within the range of volume fractions studied here. In fact, similar behaviour agreement was observed in blends of poly(amide) and EPDM-rubbers[30].

The yield stress in uniaxial tension for SAN/RH300 blends increases linearly with the logarithm of the applied strain rate (*Figure 5*). Roughly, also a linear relation of the yield stress with the rubber content can be observed (*Figure 5*). Because the pure SAN fractured before yield, the fracture stress of the homopolymer is shown in *Figure 5* for comparison.

Effect of different particles on tensile properties. The SAN/BA (40%) blends with particle size varying from 0.25 to 0.6 μm have been used to study the effect of the size of the core–shell particles on tensile properties. The results for Young's modulus and yield stress are shown in *Table 4*. As expected, the elastic modulus is nearly constant for materials with different particle sizes. Also the macroscopic uniaxial yield stress both at low and high speed does not show significant variations with particle size. This was also found in uniaxial tension experiments on HIPS[5] and in compression tests on PMMA[31].

Despite the scatter in the cavitation strain (*Table 4*), it is apparent that the RH300 and RH600 particles cavitate more easily than the UM particles, both at low as well as at high speed. According to Gent and Lindley[32], the cavitation resistance is proportional to the modulus of the particle which, in turn, is related to the network density of the rubber, through equation (4). Based on the results of the n.m.r. experiments, we can conclude that the cavitation resistance of the UM particles is higher than for RH particles, because of the difference in cross-link density.

The differences in cavitation resistance, apparently, do not cause substantial differences in the uniaxial tensile yield

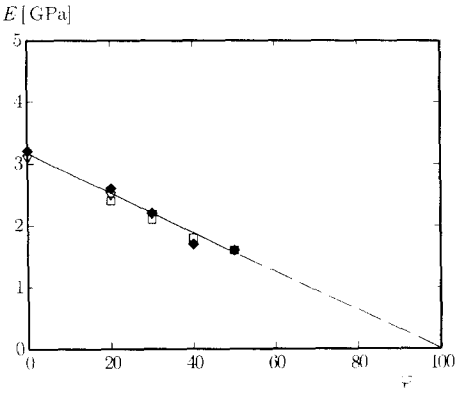

Figure 4 Young's modulus for a SAN/RH300 blends at various strain-rates as a function of rubber content: (▽) 0.001 m s^{-1}, (◆) 0.01 m s^{-1}, (□) 0.1 m s^{-1}

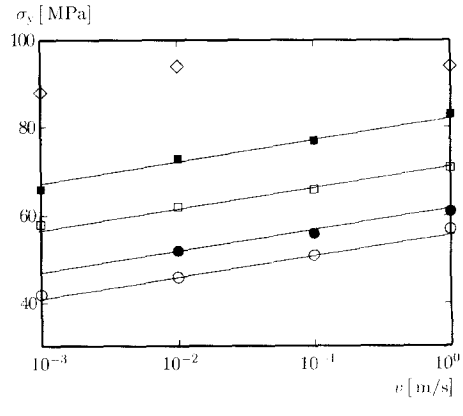

Figure 5 Yield stress as a function of strain rate for SAN/RH300 blends containing various rubber contents: (◇) 0%, (■) 20%, (□) 30%, (●) 40%, (○) 50%

Table 4 Effect of core–shell particles in SAN/BA(40%) blends on tensile properties: modulus, yield stress and cavitation strain at low and high speed

		Sample				
		UM250	RH300	UM350	UM450	RH600
Low speed (10^{-4} m s^{-1})	E (GPa)	1.52	1.60	1.56	1.56	1.60
	σ_y (MPa)	39	41	43	41	38
	ϵ_c (%)	3.8	3.3	3.3	3.9	2.9
High speed (1 m s^{-1})	σ_y (MPa)	58	58	62	62	55
	ϵ_c (%)	3.4	2.5	3.6	3.0	2.4

stress (*Table 4*). Nonetheless, the yielding in triaxial loading conditions (as in front of a crack tip) can be strongly affected, due to differences in cavitation resistance. This effect was shown in model computations[33,34], where changes in the void growth resistance of the particle (controlled by the particle stiffness), hardly reflected on the macroscopic uniaxial yield stress of the blend. In contrast, the stress at yield in a stress state with a higher triaxiality was strongly increased when the cavitation resistance was high.

Notched Izod test

The notched Izod test is used to study the effect of temperature on the fracture energy under impact conditions. As a measure for the fracture toughness, we use the brittle-to-tough transition temperature (T_{bt}). At temperatures below T_{bt}, the fracture behaviour is brittle, characterised by a low fracture energy and the absence of stress-whitening at the fracture surface. Above T_{bt}, the material is ductile, resulting in a significantly higher fracture energy, caused by massive plastic deformation and associated stress-whitening along the fracture surface. A low T_{bt} corresponds to a high fracture toughness.

First, we compare the behaviour of SAN/RH300 and SAN/RH600 blends, using rubber volume fractions between 20% and 50%. The testing temperature is varied between −40 and 80°C. The fracture energy of SAN/RH300(20%) (*Figure 6a*) is hardly affected by temperature and behaves in a brittle manner. For SAN/RH300 blends with rubber volume fraction of 30% and higher, a sharp brittle-to-tough transition is observed upon variation of the testing temperature. With increasing rubber content the T_{bt} decreases.

The SAN/RH600 blends (*Figure 6b*) show an increasing fracture energy with increasing temperature, but brittle-to-tough transitions are not as a sharp as in the case of SAN/RH300 materials. A prerequisite for a sharp brittle–tough transition is a well-defined morphology (regular particle size and particle distribution). On the basis of the notched Izod test, one may speculate that the microstructure of the SAN/RH600 blends is not as regular as for the SAN/RH300 blends. However, this cannot be deduced from the TEM morphology studies. Nonetheless, SAN/RH600 blends have a lower T_{bt}, compared to SAN/RH300, suggesting that the larger particles provide somewhat better toughening.

Next, the results of notched Izod impact test with SAN/UM(40%) materials are compared with those of the SAN/RH(40%) series. If the particle size is the controlling factor for fracture toughness, it should be expected that the SAN/UM blends have a T_{bt} that is between the T_{bt} of SAN/RH300 and of SAN/RH600 blends, since the particle size is in the same range. For the SAN/UM(40%) materials no significant toughening effect is observed over the entire temperature range (*Figure 7*). Since the morphology and particle size of the SAN/RH and SAN/UM blends are similar, it is most

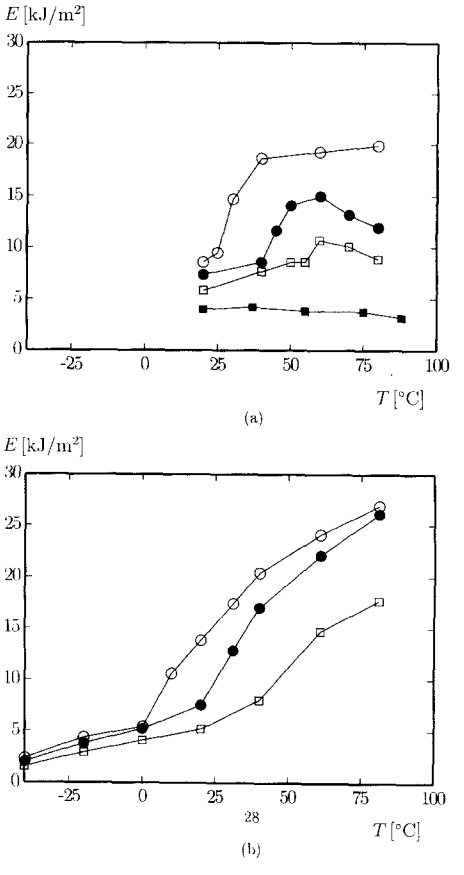

Figure 6 Notched Izod impact fracture toughness as a function of temperature for SAN/BA core shell rubber blends containing various rubber contents: (■) 20%, (□) 30%, (●) 40%, (○) 50%). (*a*) SAN/RH300 blends, particle size 0.3 μm; (*b*) SAN/RH600 blends, particle size 0.6 μm

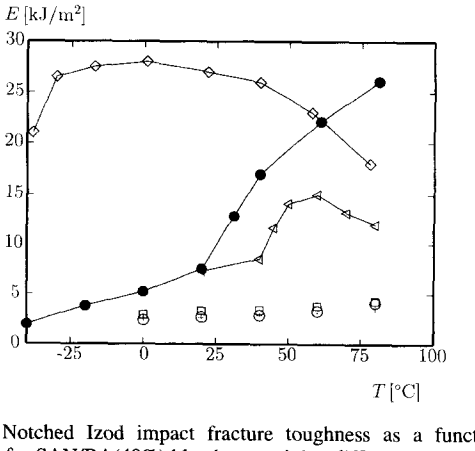

Figure 7 Notched Izod impact fracture toughness as a function of temperature for SAN/BA(40%) blends, containing different types of core–shell particles and SAN/PB(40%) for comparison [9]: (◁) RH300, (●) RH600, (○) UM250, (+) UM350, (□) UM450, (◇) PB

likely that the differences in impact fracture toughness are caused by the differences in the mechanical properties of the particles. The rubbery phase of the UM particles has a network density about three times as high as in the case of the RH particles. As a consequence, the modulus and therefore the cavitation resistance of the UM particles is higher. If the cavitation resistance is high, the plastic deformation processes are suppressed and the energy dissipation during fracture is reduced.

It is noted that the toughening efficiency for the materials discussed here is significantly lower than for blends of SAN with poly(butadiene) (PB)[9]. In that study, the results of impact fracture experiments for a SAN/PB(30%) blend (a SAN TYRIL 790, DOW and 0.1 μm PB core–shell particles GRC 310, DOW) are reported. The T_{bt} in a notched Izod test for that blend was found to be −40°C, which is much lower than the T_{bt} found in this study. We do not have experimental data for the properties of the poly(butadiene) core, except that for PB $T_g \approx -80$°C at 1 Hz, which is much lower than that for BA. Therefore, we assume that the cavitation resistance of the PB core–shell particles at low temperatures and under impact conditions is much lower than for the BA particles studied here, which could explain the higher toughness. The foregoing results indicate that rubber-toughening of SAN is very sensitive to the properties of the rubber particle.

Notched tensile test

The fracture energy of SAN/BA(40%) blends is measured by means of a notched tensile test, both at low speed (10^{-4} m s^{-1}) and at high speed (1 m s^{-1}). The temperature is varied between 20 and 90°C.

For both speeds, maximum load and fracture energy are shown as a function of temperature in *Figure 8*. At 10^{-4} m s^{-1}, the maximum force decreases with increasing temperature for all materials. The differences in maximum force for the various materials are significantly smaller than in the case of the yield stress in the unnotched tensile test. The fracture energy for SAN/RH blends is higher than for SAN/UM materials, except for temperatures higher than 70°C, where a strong increase in fracture energy occurs for SAN/UM250 and SAN/UM450. At high tensile speed (1 m s^{-1}), the maximum load for SAN/RH materials is clearly higher than for SAN/UM materials. The total

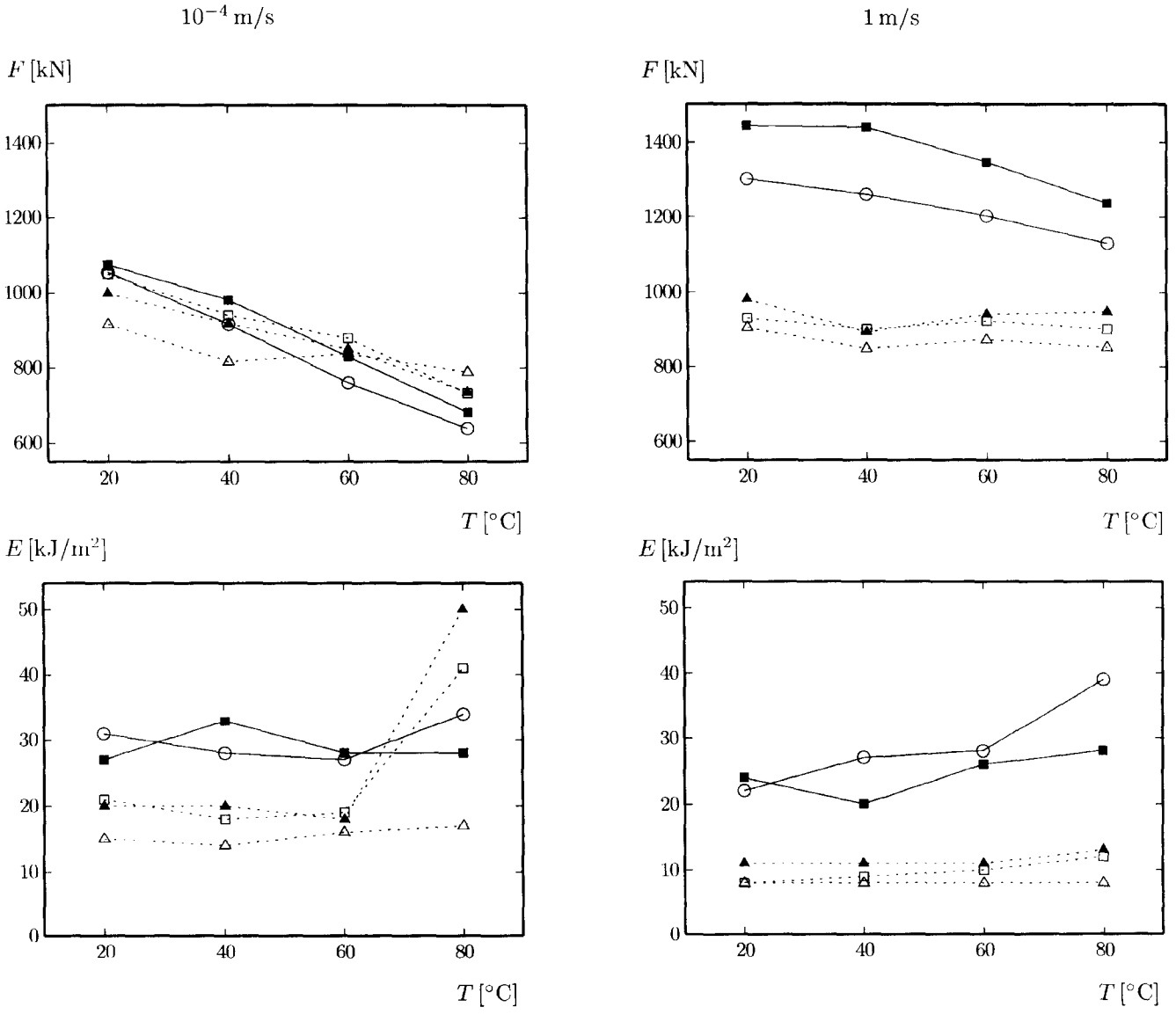

Figure 8 Maximum load and total fracture energy in the notched tensile test, for SAN/BA(40%) blends. The results are given for low speed (10^{-4} m s^{-1}) and high speed (1 m s^{-1}) as a function of temperature: (■) RH300, (○) RH600, (□) UM250, (△) UM350, (▲) UM450

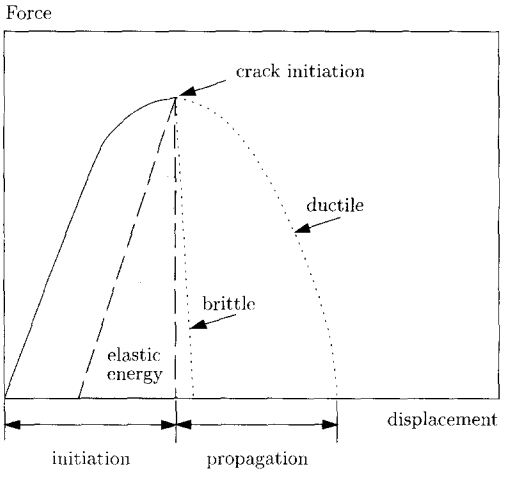

Figure 9 Schematic representation of typical force–displacement curves from the notched tensile test, and characterization of the fracture behaviour

fracture energy for the SAN/RH materials is higher than for SAN/UM materials.

From the foregoing results it is difficult to classify the fracture behaviour into either brittle or tough, in the way it is done for the notched Izod test. However, during the notched tensile test, the tensile force and clamp displacement are accurately monitored, which facilitates a more advanced examination of the fracture behaviour. Two idealised situations are considered here, referred to as either brittle or ductile fracture, which are illustrated in *Figure 9*. It is assumed that crack initiation occurs at maximum load. The propagation energy is defined as the area under the force–displacement curve after maximum load. When the propagation energy is very low compared to the total energy, the material is termed brittle. This fracture mode is typically unstable, i.e. the energy release upon crack advancement is sufficient to drive further crack growth. If, on the other hand, considerable energy dissipation takes place during fracture, the propagation energy cannot be neglected compared to the total energy, and the fracture mode is called ductile. These considerations lead to a convenient way to characterize the fracture toughness; by using the ratio of propagation energy E_{prop} and total fracture energy E_{tot}.

This ratio, $(E_{prop})/(E_{tot})$, is plotted in *Figure 10* for the SAN/BA(40%) blends. At low speed (10^{-4} m s^{-1}), the fracture toughness for SAN/RH300 and SAN/RH600 materials increases with increasing temperature. The SAN/UM materials are brittle except for SAN/UM250 and SAN/UM450 which show a brittle–tough transition at 80°C. At high speed (1 m s^{-1}), all blends studied show brittle fracture up to 60°C. SAN/RH600 has a brittle–tough transition at 70°C. Qualitatively, these results are in good agreement with the notched Izod experiments; the SAN/RH blends have a higher fracture toughness than the SAN/UM materials. This is caused by the higher cavitation resistance for UM particles, due to a higher network density. The toughening efficiency of RH600 particles in SAN seems to be slightly better than using RH300 particles. Here, we note again that the fracture energy in the notched tensile test for the SAN/BA blends is much lower than that for the SAN/PB blends[9].

CONCLUSIONS

The toughening effect of various core–shell particles has been investigated using styrene–acrylonitrile as a matrix. The size of the poly(butyl-acrylate) core and poly(methyl-methacrylate) shell particles was varied from 0.1 to 0.6 μm in diameter. The smallest particles (0.1 and 0.15 μm) cannot be mixed in without severe clustering of the particles. Larger particles were dispersed quite well in the matrix.

From n.m.r. experiments, it follows that the network density of the rubber core of the UM particles is three times as high as for RH particles. Consequently, the cavitation resistance for UM particles is higher than for RH particles.

The elastic modulus and yield stress of the blends are independent on particle properties and size. The cavitation strain of SAN/RH blends is lower than for SAN/UM blends.

The notched Izod impact toughness of SAN/BA blends is

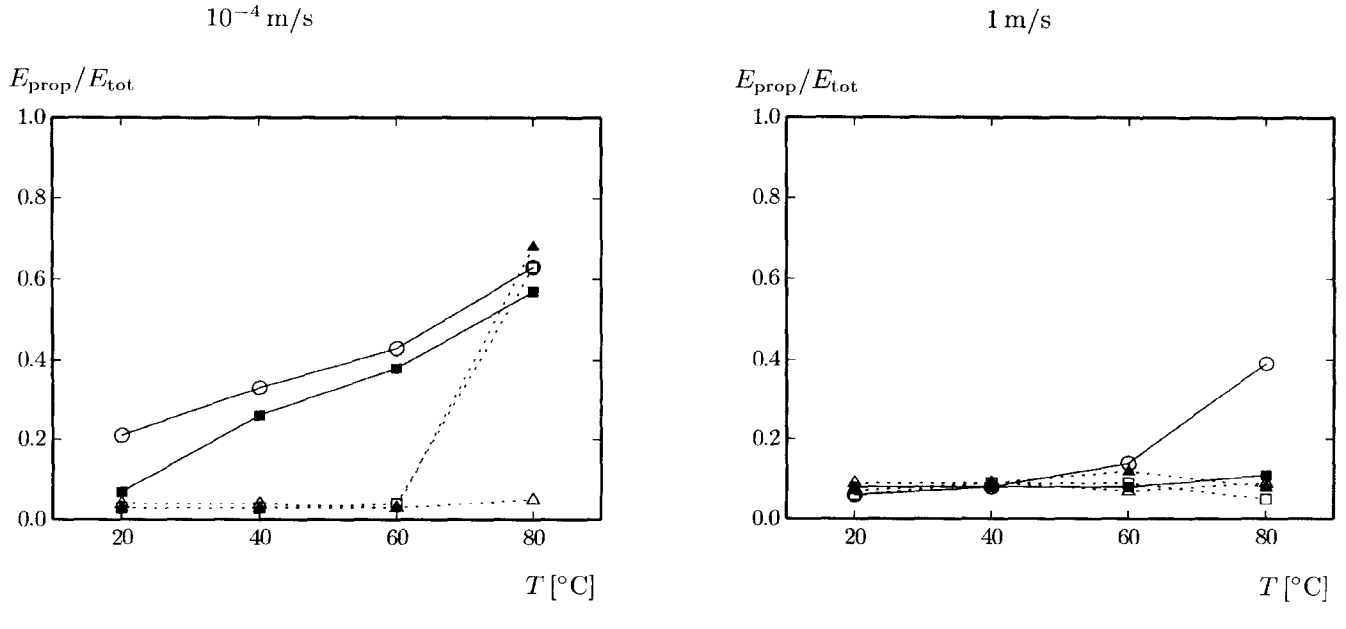

Figure 10 Propagation energy relative to the total fracture energy in the notched tensile test, for SAN/BA(40%) blends. The results are given for low speed (10^{-4} m s^{-1}) and high speed (1 m s^{-1}) as a function of temperature: (■) RH300, (○) RH600, (□) UM250, (△) UM350, (▲) UM450

very sensitive to the properties of the rubber particle. Between 20 and 90°C all the blends with UM particles were brittle, whereas the blends with RH particles showed a brittle-to-tough transition. The brittle-to-tough transition temperature for the blends with larger particles (0.6 μm) is lower than for the blends with smaller particles (0.3 μm), suggesting a weak particle size effect.

These results are qualitatively confirmed in a notched tensile test, both under quasi-static loading (10^{-4} m s^{-1}), and under impact conditions (1 m s^{-1}). A low cavitation resistance of the rubber particles appears to be crucial to achieve a high toughening efficiency.

ACKNOWLEDGEMENTS

The work of A.C. Steenbrink is part of a research project funded by The Netherlands Technology Foundation (STW). The authors would like to thank A.C. van der Sluis for his contribution to this work.

REFERENCES

1. Bucknall, C. B., *Toughened Plastics*, Applied Science Publishers, London, 1977.
2. Donald, A.M. and Kramer, E.J., *J. Appl. Pol. Sci*, 1982, **27**, 3729–3741.
3. Hobbs, S.Y., *Pol. Eng. Sci.*, 1986, **26**, 74.
4. Liu, N.C. and Baker, W.E., *Pol. Eng. Sci.*, 1992, **32**, 1695.
5. Bucknall, C.B., Davies, P. and Partridge, I.K., *J. Mat. Sci.*, 1987, **22**, 1341–1346.
6. Borggreve, R.J.M. and Gaymans, R.J., *Polymer*, 1989, **30**, 63.
7. Seo, Y., Hwang, S.S., Kim, K.U., Lee, J. and Hong, S.I., *Polymer*, 1993, **34**, 1667.
8. Cook, D.G., Rudin, A. and Plumtree, A., *J. Appl. Pol. Sci.*, 1993, **48**, 75.
9. Steenbrink, A. C., Gaymans, R. J. and van der Giessen, E., *Preprints Polymat Conference*, London, Sept. 1994, p. 598.
10. Dompas, D., Groeninckx, G., Isogawa, M., Hasegawa, T. and Kadokura, M., *Polymer*, 1995, **36**, 437.
11. Breuer, H., Haaf, F. and Stabenow, J., *J. Macromol. Sci.-Phys.*, 1977, **14**, 387.
12. Bubeck, R.A., Buckley, D.J., Kramer, E.J. and Brown, H., *J. Mat. Sci.*, 1991, **26**, 6249.
13. Ramsteiner, F. and Heckmann, W., *Polymer Commun.*, 1985, **26**, 199.
14. Lazzeri, A. and Bucknall, C.B., *J. Mat. Sci.*, 1993, **28**, 6799.
15. Dijkstra, K.D., Van der Wal, A. and Gaymans, R.J., *J. Mat. Sci.*, 1994, **29**, 3489–3496.
16. Yee, A.F. and Pearson, R.A., *J. Mat. Sci.*, 1986, **21**, 2462.
17. Gent, A.N. and Tompkins, D., *J. Pol. Sci. Part A-2*, 1969, **7**, 1483.
18. Datasheet TYRIL, Dow Chemical Co.
19. Van Krevelen, D. W., *Properties of Polymers*, 3rd edn. Elsevier, 1990.
20. Montezinos, D., Wells, B.G. and Couchman, P.R., *Macromolecules*, 1983, **16**, 589.
21. Farrar, T. C. and Becker, E. D., *Pulse and Fourier Transform NMR. Introduction to Theory and Methods*. AP, New York, 1971.
22. MacBrierty, V. J. and Packer, K. J., *Nuclear Magnetic Resonance in Solid Polymers*, Cambridge University Press, 1993.
23. Gotlib, Yu.Y., Lifhits, M.I., Shevelev, V.A., Lishanskii, I.S. and Balanina, I.V., *Polym. Sci. USSR*, 1976, **A18**, 2630.
24. Fry, C.G. and Lind, A.C., *Macromolecules*, 1988, **21**, 1292.
25. V.M. Litvinov, W. Barendswaard, M. van Duin, to be published.
26. Béguelin, Ph., Ph.D. Thesis, École Polytechnique Fédérale de Lausanne, 1996.
27. Tsvetkov, V.N., Boitsova, N.N. and Vitovskaya, M.G., *Polym. Sci. USSR*, 1964, **6**, 341.
28. Kim, H., Keskkula, H. and Paul, D.R., *Polymer*, 1991, **32**, 1447.
29. Hill, R., *J. Mech. Phys. Sol.*, 1963, **11**, 357–372.
30. Borggreve, R.J.M., Gaymans, R.J., Schuijer, J. and Ingen Housz, J.F., *Polymer*, 1987, **28**, 1489.
31. Gloaguen, J.M., Heim, P., Gaillard, P. and Lefebvre, J.M., *Polymer*, 1992, **33**, 4741.
32. Gent, A.N. and Lindley, P.B., *Proc. Roy. Soc. London*, 1958, **A249**, 195–201.
33. Steenbrink, A. C. and van der Giessen, E., in *5th European Symposium on Polymer Blends*, Maastricht, May 1996, p. 254.
34. Steenbrink, A. C., van der Giessen, E. and Gaymans, R. J., in *MI Conference on Deformation, Yield and Fracture of Polymer Blends*, 7–10 April 1997, Cambridge, UK.